Preprint
UCRL-JC-147866

Ti-Cr-Al-O Thin Film Resistors

A. F. Jankowski, J. P. Hayes

This article was submitted to
The International Conference on Metallurgical Coatings and Thin Films, San Diego, CA., April 22-26, 2002

March 21, 2002

U.S. Department of Energy

Lawrence
Livermore
National
Laboratory

This work was performed under the auspices of the United States Department of Energy by the University of California, Lawrence Livermore National Laboratory under contract No. W-7405-Eng-48.

Ti-Cr-Al-O Thin Film Resistors

Alan F. Jankowski and Jeffrey P. Hayes

Lawrence Livermore National Laboratory, P.O. Box 808, Livermore, CA 94550

Abstract

Thin films of Ti-Cr-Al-O are produced for use as an electrical resistor material. The films are rf sputter deposited from ceramic targets using a reactive working gas mixture of Ar and O_2. Vertical resistivity values from 10^4 to 10^{10} Ohm-cm are measured for Ti-Cr-Al-O films. The film resistivity can be design selected through control of the target composition and the deposition parameters. The Ti-Cr-Al-O thin film resistor is found to be thermally stable unlike other metal-oxide films.

Introduction

In one microelectronics application of metal-oxide materials, thin films are used for electrically resistive elements. Often, ceramic-metal composites, i.e. cermets, as Cr-Si-O are sputter deposited using varying target compositions with multiple phases as a path to change the resistance by many orders of magnitude. [1-5] The conduction mechanism for the Cr-Si-O cermets can be considered quantum mechanical. [6] At low metallic concentrations the charge transport can be modeled using the effective medium theory in which electron tunneling occurs between metallic particles dispersed in an insulating medium. [7] In general, conduction occurs by means of an activated charge transport process. For film resistivity values greater than 10^{-2} Ω cm, the Cr-Si-O cermet microstructure is comprised of a continuous insulating SiO_2 matrix in which Cr and its silicides-monoxides serve as the conductors/semiconductors. Recently, the effective medium theory is used to account for the behavior of Cr-Si-O over a wide range of vertical resistivity values from 10^1 to 10^{14} Ω cm and the rapid increase in resistivity as the film composition increases to 80 vol.% SiO_2. [8-9]

A concern does arise with respect to the thermal stability of the Cr-Si-O cermet material. Specifically, low temperature anneal cycles can significantly affect the resistivity value of the film and its performance. [9] For example, a 2 hr anneal at 450 °C is shown to increase the resistivity of Cr-Si-O by an order of magnitude. At present, there is interest in developing a thermally stable, metal-oxide material for use as a lateral or vertical resistor as, for example, a layer beneath a field emission cathode in a flat panel display. The Ti-Cr-Al-O material system is identified for this resistor application. [10-11] In addition, the Ti-Cr-Al-O metarial can be used to control the surface emission of secondary electrons as, for example, a thin coating on an insulating material such as a vertical wall support in a flat panel display. The need for thermal stability arises as post deposition processing of the electronic components can reach temperatures of several hundred degrees centigrade.

Experimentals

The Ti-Cr-Al-O coatings are sputter deposited from 6.4 cm diameter, ceramic targets using planar magnetrons operated in the rf mode with forward powers up to 7 W cm^{-2}. The sputter targets used are a hot-isostatic pressing of ceramic powder precursors. A blend of TiO_2, Al_2O_3, and Cr_2O_3 powders is mixed to yield the desire composition of the sputter target. The titania (rutile TiO_2) component is varied in substitution with respect to a constant ratio of alumina (corundum Al_2O_3) and chromia (corundum Cr_2O_3). The target composition is expressed in weight percent (wt.%) as $[(Al_2O_3)_{35}(Cr_2O_3)_{65}]_{100-x}(TiO_2)_x$. Target compositions (x) of 1.73, 7, 10, and 14 wt.% TiO_2 are used in sputter deposition of the coatings. The film thickness (t) must be sufficient to avoid the effects seen for films thinner than 0.1 μm. [12-13] So, the Ti-Cr-Al-O coatings are deposited in a range of thickness from 0.2 to 1.2 _m. A working gas mixture of (1-z)Ar-(z)O_2 (where z < 0.08) is controlled by flow (q_{Ar-O_2}) over a range of 32-115 cc-min^{-1} at pressures (p_{Ar-O_2}) of 0.4-4.0 Pa. For reference, the deposition system base pressure is on the order of 10^{-6} to 10^{-7} Pa. To account for the residual presence of oxygen when sputtering with pure Ar, it's assumed (in an overestimation) that the oxygen partial pressure is equal to 20% of the system base pressure. The substrates are silicon wafers that are first sputter-coated with 0.3 μm of Ni-7 wt.% V. This base layer serves as the bottom metal contact for the vertical resistance measurement. A 10 cm source-to-substrate separation is used and a rise in substrate temperature to 75 °C can occur during deposition. Deposition rates vary from 0.001 to 0.02 nm W^{-1} min^{-1} depending upon the sputter gas mixture and pressure as well as the target composition. To assess the thermal stability of the films, anneals are performed in air as well as under vacuum (at 10^{-5} Pa). The samples are heated at a rate of 20 °C min to a maximum temperature of 400 °C, held at the desired temperature for 2 hr., and then cooled to room temperature at a rate of 30 °C min.

The elemental composition (at.%) of the Ti-Cr-Al-O film is determined using Rutherford Backscattering (RBS). The films are analyzed using 2.3 MeV He^+ ions at normal incidence with a 4 mm^2 beam spot at a 164° detection angle. In addition, particle-induced x-ray emission (PIXE) spectra were collected to provide enhanced elemental specificity. The ultra-thin windowed x-ray detector was located at a 150° detection angle. The absolute number of He^+ ions generating each spectrum was determined by a spinning-wire dosimetry system. [14] The RBS spectra consist of well-separated signals for Ti, Cr, Al and O with essentially no background under the elemental signals. The relative intensity counts from each of the elements is determined with high precision (<1%) and quantifiable through the surface approximation. [15] Although the surface approximation slightly overestimates the actual number of atoms cm^{-2}, an accurate measure of the relative atomic concentrations (±1%) is made without requiring knowledge of the stopping cross-sections for the film. An assessment of the crystalline structure in the coatings is made using x-ray diffraction. A rotating-anode source operated at 40 keV and 200 mA illuminates the coatings with Cu $k\alpha$ radiation in the $\theta/2\theta$ mode. It should be noted that x-ray diffraction characterization of sputter-deposited oxide coatings often yields diffuse Bragg reflections that can make phase identification difficult in nanocrystalline or amorphous coatings.

A test method is developed for measuring the current (I) versus voltage (V) behavior of the sputter deposited films that yields a unique and reproducible resistivity value. [8-9] The resistive path through the film thickness is measured between contact pads using a semiconductor parameter analyzer. A square array (5 mm x 5 mm) of four, molybdenum (Mo) contact pads (254 μm diameter x 0.5 μm) are electron-beam deposited onto the Ti-Cr-Al-O films. The current is measured as a potential is applied from zero to 20 V in 200 mV increments. Each of the four Mo contact pad combinations are used to produce independent measures of resistance. The resistive path is through twice the film thickness, i.e. from the first top-contact pad to the bottom-contact Ni-V layer and back to the second top-contact pad. The vertical resistance (ρ) is determined from the field (E) and current density (J) using the standard expressions [9]

$$\rho = E\,(J)^{-1}, \tag{1}$$

where

$$E = V\,(2t)^{-1}, \tag{2}$$

and

$$J = I\,(A_c)^{-1} \tag{3}$$

noting that (A_c) is the contact area between each Mo pad and the Ti-Cr-Al-O film surface.

Results and Analysis

The characteristic, current-voltage behavior of the coatings is shown (in Fig. 1) for deposits from the 7 wt.% and 10 wt.% TiO_2 targets. The 0.64 _m thick coating from the 7 wt.% TiO_2 target is deposited using a 0.8 Pa working gas pressure ($p_{Ar\text{-}O_2}$) with an O_2 partial pressure (p_{O_2}) of 3.2 mPa. The 0.46 _m thick coating from the 10 wt.% TiO_2 target is deposited using a $p_{Ar\text{-}O_2}$ of 0.8 Pa with a p_{O_2} of 2.0 mPa. In general, the current-voltage behavior is approximately linear beyond an applied potential of 5 V. The current-voltage behavior of the samples appears to be quite stable with respect to thermal annealing. The as deposited coating from the 7 wt.% target has a resistivity of 1.0 $\times 10^5$ Ω cm that does not change after a 2 hr vacuum anneal at 250 °C and then increases 10 % to 1.1 $\times 10^5$ Ω cm after a subsequent 2 hr air anneal at 150 °C. The as deposited coating from the 10 wt.% target has a resistivity of 2.4 $\times 10^5$ Ω cm that increases 10 % to 2.7 $\times 10^5$ Ω cm after a 2 hr air anneal at 300 °C and then increases to just 2.8 $\times 10^5$ Ω cm after a subsequent 2 hr vacuum anneal at 350 °C. Coatings with greater intrinsic resistivity appear to be equally as stable. A 0.53 _m thick coating from the 10 wt.% TiO_2 target is deposited using a $p_{Ar\text{-}O_2}$ of 0.8 Pa with a nominal background p_{O_2} of 3.5 $\times 10^{-3}$ mPa. This as deposited coating from the 10 wt.% target has a resistivity of 3.2 $\times 10^8$ Ω cm that increases to 3.25 $\times 10^8$ Ω cm after a 2 hr air anneal at 300 °C, then decreases to 3.1 $\times 10^8$ Ω cm subsequent to a 2 hr vacuum anneal at 350 °C.

The sputter gas composition affects the resistivity of the coating. A series of curves (seen in Fig. 2) shows the decrease in resistivity by more than four orders of magnitude from 10^9 to 10^5 Ω cm that occurs with an increase of the O_2 partial pressure in the sputter gas mixture at a total Ar-O_2 working gas pressure of 0.8 Pa. The curves for these coatings deposited from the 7 wt.% target are typical for the entire series of Ti-Cr-Al-O deposits. A linear variation of $\log_{10}(\rho)$ with voltage is observed with a near constant value for ρ beyond an applied potential of 5 V.

The deposition rate affects the resistivity of the coating as seen in a plot (Fig. 3) of the vertical resistivity measured for all of the coatings deposited from all of the (1.73, 7, 10, and 14 wt. % TiO_2) targets under all process conditions of gas composition and pressure. Several of these samples deposited from the 7 and 10 wt.% TiO_2 targets are listed in Table 1 along with corresponding RBS measurements of elemental composition. Although there is scatter in the data of Fig. 3, the merit of this plot is seen in the general trend that the $\log_{10}(\rho)$ increases linearly with an increase in the deposition rate. Noting that the deposition rate increases as the p_{O_2} decreases during the sputtering process, less oxygen in the sputter gas yields films with greater resistivity as seen in the Fig. 2 results.

The effect of the p_{O_2} on the resistivity for all of the coatings under all deposition conditions is shown in Fig. 4. An increase in the $\log_{10}(p_{O_2})$ above 10^{-3} Pa results with an inversely proportional decrease in $\log_{10}(\rho)$ from 10^7-10^{11} Ω cm to a baseline value of 3×10^4 Ω cm. There is little change in ρ below a p_{O_2} of 10^{-3} Pa. The results for the baseline p_{O_2} conditions of deposition may illustrate the effect of target composition over the upper bound to the resistivity range from 10^7 to 10^{11} Ω cm. A plot of the TiO_2 content versus ρ (as shown in Fig. 5 for depositions with a p_{O_2} less than 10^{-5} Pa) reveals a minimum in the resistivity value for the 10 wt.% target. The ρ increases both above and below the 10 wt.% target composition. An optimal TiO_2 content may appear for producing the most conductive Ti-Cr-Al-O film. The correlation between the elemental composition (shown in Table 1) and the vertical resistivity of the coating appears in general trends alone. The resistivity tends to increase as the Cr content increases and as the Al decreases. A local maximum may appear in the Ti content and a local minimum may appear in the O content of the films that correspond with a 10^7 _ cm resistivity.

The $\theta/2\theta$ x-ray diffraction spectra taken of two 7 wt.% TiO_2 coatings that are listed in Table 1, i.e. samples no. 603 and 625, are shown in Fig. 6. These samples are of generic interest since the measured resistivity differs by a multiple of 10^4 between the coatings. The diffraction characterization can provide insight to the microstructure that corresponds with this large difference in resistivity. The 2θ positions of the Bragg reflections from each coating spectra are listed in Table 2 along with the characteristic Miller indices (hkl) for the reflections of the material phases within the sputter target, the substrate, and the base layer. All of the Bragg reflections can be attributed to these material phases. The reflections of the Si substrate, its native oxide, and the Ni-V base layer appear in the diffraction scans of both coatings no. 603 and 625. The characteristic reflections of each oxide phase, i.e. the rhombohedral structure of the Al_2O_3 and Cr_2O_3 corundum phases along with the tetragonal structure of the TiO_2 rutile phase, are found in the remaining reflections. A match is only considered if the computed (hkl) interplanar spacings of the known phase and the measured reflection differ by 1% or less. Also, there is a possibility that some of the elemental metal species exist in the coatings. For example, the Cr (110) and (200) coincide with the Ni (111) and Cr_2O_3 (300), respectively. The x-ray diffraction characterization indicates that there is a well-defined crystalline component to each coating. The more resistive coating no. 603 evidences a Cr_2O_3 (012) reflection that is not found in the less resistive coating no. 625. Similarly, the less resistive coating no. 625 evidences a Al_2O_3 (012) reflection with a broad half-width that is not found in the more resistive coating no. 603. Unique but different TiO_2 reflections are found for each coating, i.e. a (110) in no. 603 and a (211) with a broad half-width in no. 625. From these results, it can be speculated that the Bragg reflections with a broad half-width correspond with nanocrystalline phases in the lower resistivity coating (no. 625) that was deposited with an Ar-O_2 gas mixture as opposed to the greater resistivity coating (no. 603) that was deposited with nominally pure Ar. In general, x-ray diffraction characterization does reveal the presence of crystalline phases that correspond with the target material. However, it's not clear that a distinction as to what role the matrix phases of target material, i.e. Al_2O_3, Cr_2O_3 or TiO_2, have in determining the resistivity behavior.

Discussion and Summary

The stability of the Ti-Cr-Al-O coating reflects its inherent nature as a ceramic blend rather than as a cermet composite. As previously mentioned, Cr-Si-Oxide films sputter deposited from $Cr\text{-}Cr_2O_3\text{-}SiO_n$ targets are shown to be thermally unstable. [8-9] Low temperature anneals are known to phase separate the Cr-Si-O matrix into coarsened metal-rich particles that results with a factor of 10 increase in the resistivity. In contrast to cermets, the Ti-Cr-Al-O films remain stable after thermal annealing with small changes in ρ that are less than 10%. The nature of the conduction mechanism in the Ti-Cr-Al-O does not appear to follow the trends observed for cermet materials as Cr-Si-O in which metallic particulates are dispersed throughout an insulating matrix. Further investigation will be required to clarify the conduction mechanism in the Ti-Cr-Al-O system as, for example, through low-temperature resistivity measurements.

In summary, crystalline Ti-Cr-Al-O films are reactively deposited from $[(Al_2O_3)_{35}(Cr_2O_3)_{65}]_{100-x}(TiO_2)_x$ targets where x equals 1.73, 7, 10, and 14 wt.% using an $Ar\text{-}O_2$ sputter gas mixture. The vertical resistivity (ρ) of the coatings is found to be thermally stable when cycled to 400 °C in air or vacuum. A wide range of ρ values is produced in the Ti-Cr-Al-O system from 10^4 to 10^{11} Ω cm. The $\log_{10}(\rho)$ is found to increase linearly with deposition rate. Also, the $\log_{10}(\rho)$ increases inversely proportionate to a decrease in $\log_{10}(p_{O_2})$. The effect of target composition is pronounced for deposits using a working gas of nominally pure Ar, in which a local minimum of ρ at 10^7 Ω cm is found for the 10 wt.% TiO_2 composition. The Ti-Cr-Al-O ceramic system offers promising use in applications as flat panels displays that require thermally stable, vertical and lateral resistor layers.

Acknowledgments

The authors thank R. Musket and D. del Giudice for their contributions to the RBS and x-ray diffraction measurements, respectively. This work was performed under the auspices of the U.S. Department of Energy by University of California, Lawrence Livermore National Laboratory under contract No. W-7405-Eng-48.

References

1. C. A. Neugebauer, Thin Solid Films, 6 (1970) 443
2. R. Glang, R. A. Holmwood and S. R. Herd, J. Vac. Sci. Technol., 4 (1967) 163
3. A. A. Milgram and C-S. Lu, J. Appl. Phys., 39 (1968) 4219
4. N. C. Miller and G. A. Shirn, Solid State Tech., 11 (1968) 28
5. H. Steemers and R. Weisfield, Mater. Res. Soc. Symp. Proc., 118 (1988) 445
6. J. E. Morris, Thin Solid Films, 11 (1972) 299
7. B. E. Springett, J. Appl. Phys., 44 (1973) 2925
8. A.F. Jankowski, J.P. Hayes, R.G. Musket, F. Cosandey, C.E. Gorla, R.S. Besser, V. Westerlind and G. Cobai, in E. Ma, B. Fultz, R. Schull, J. Morral and P. Nash (eds.) Chemistry and Physics of Nanostructures and Related Non-Equilibrium Materials, TMS Symposia Proceedings, Metals Park, OH, 1997, p. 211
9. A. Jankowski, Thin Solid Films, 332 (1998) 272
10. A.F. Jankowski and A.P. Schmid, Ti-Cr-Al-O Thin Film Resistors, U.S. Patent No. 6,154,119 (Nov. 28, 2000)

11. A.F. Jankowski and A.P. Schmid, Process for Producing Ti-Cr-Al-O Thin Film Resistors, U.S. Patent No. 6,217,722 (Apr. 17, 2001)
12. T. Filutowicz, W. Gregorczyk and B. Stepien, Electron Technology, 10 (1977) 117
13. H. S. Hoffman and E. Stephans, IEEE Trans. on Components, Hybrids and Manufacturing Technol., 4 (4) (1981) 387
14. R. G. Musket, R. S. Daley and R. G. Patterson, Nucl. Instr. and Meth., B83 (1993) 425
15. RUMP program, Computer Graphics Service, Lansing, NY 14882, USA

Table I. – The resistivity (Ohm-cm) and composition (at.%) of Ti-Cr-Al-O coatings

Sample	x (wt.%)	$p_{Ar\text{-}O_2}$ (Pa)	p_{O_2} (Pa)	Ti (at.%)	Cr (at.%)	Al (at.%)	O (at.%)	_ (_ cm)
603	7	2.0	3.5×10^{-6}	2.2	21.2	17.0	59.6	1.5×10^{9}
604	7	0.8	2.7×10^{-6}	1.5	20.1	17.7	60.7	7.0×10^{8}
606	7	0.8	3.2×10^{-3}	1.9	20.0	17.2	60.9	1.5×10^{6}
625	7	0.8	4.8×10^{-3}	2.0	17.5	18.8	61.7	2.4×10^{5}
628	7	0.8	6.0×10^{-3}	1.9	16.2	19.5	62.3	1.6×10^{5}
729	7	0.4	4.7×10^{-6}	2.0	19.2	18.1	60.7	1.9×10^{9}
711	10	2.0	3.2×10^{-6}	2.0	18.3	18.0	61.5	5.0×10^{9}
717	10	2.0	2.0×10^{-1}	2.0	20.5	9.4	68.1	3.0×10^{4}
720	10	2.0	1.3×10^{-6}	2.5	18.0	19.0	60.2	4.0×10^{7}
905	10	2.0	1.3×10^{-1}	2.1	19.6	10.0	68.3	3.0×10^{4}
124	10	0.8	4.8×10^{-3}	2.0	17.4	18.5	62.1	3.0×10^{5}
126	10	0.8	6.0×10^{-3}	1.5	17.4	18.8	62.3	5.0×10^{4}
130	10	0.8	7.5×10^{-3}	2.0	15.7	20.0	62.3	3.0×10^{4}
201	10	0.8	3.2×10^{-3}	2.3	20.3	19.2	58.2	1.5×10^{6}

Table II. – The 2θ Bragg reflections (degrees) and matching phases of Ti-Cr-Al-O coatings							
$2\theta_{603}$	$2\theta_{625}$	Si	SiO_2	Ni(V)	Al_2O_3	Cr_2O_3	TiO_2
22.02	22.22		**(1 0 1)**				
24.64	-					**(0 1 2)**	
-	25.55				**(0 1 2)**		
28.14	-						**(1 1 0)**
32.82	32.85	**(2 0 0)**					
33.74	33.76					**(1 0 4)**	
37.94	37.95				**(1 1 0)**		
41.33	41.41				(0 0 6)	(1 1 3)	(1 1 1)
44.21	44.22			**(1 1 1)**		(2 0 2)	(2 1 0)
51.82	51.92			**(2 0 0)**	(0 2 4)		
-	53.47						**(2 1 1)**
61.63	61.62				**(0 1 8)**		
64.59	64.59					(3 0 0)	(3 1 0)
69.03	69.04	**(4 0 0)**			(3 0 0)		(3 0 1)
74.34	74.36				(2 0 8)		(3 2 0)
77.74	77.73			**(2 2 0)**	(1 1 9)	(2 2 0)	

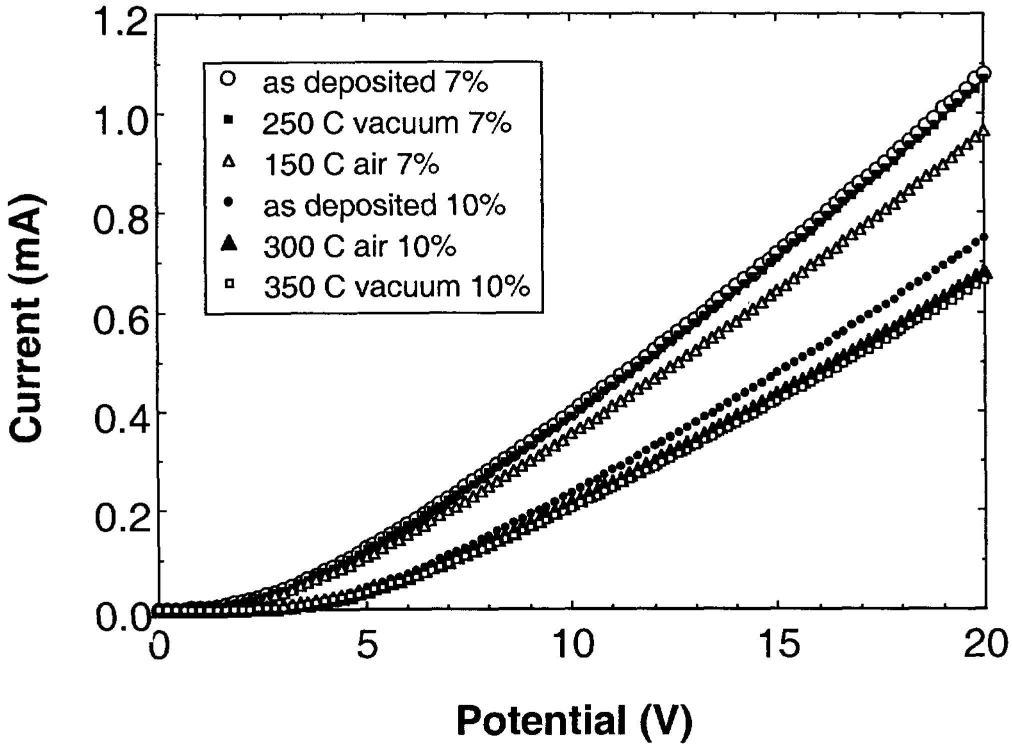

Figure 1. – The variation of current (mA) with the applied potential (V) for coatings sputter deposited from the 7 and 10 wt.% TiO_2 targets are plotted as measured in the as-deposited condition and after thermal anneals in air as well as in vacuum.

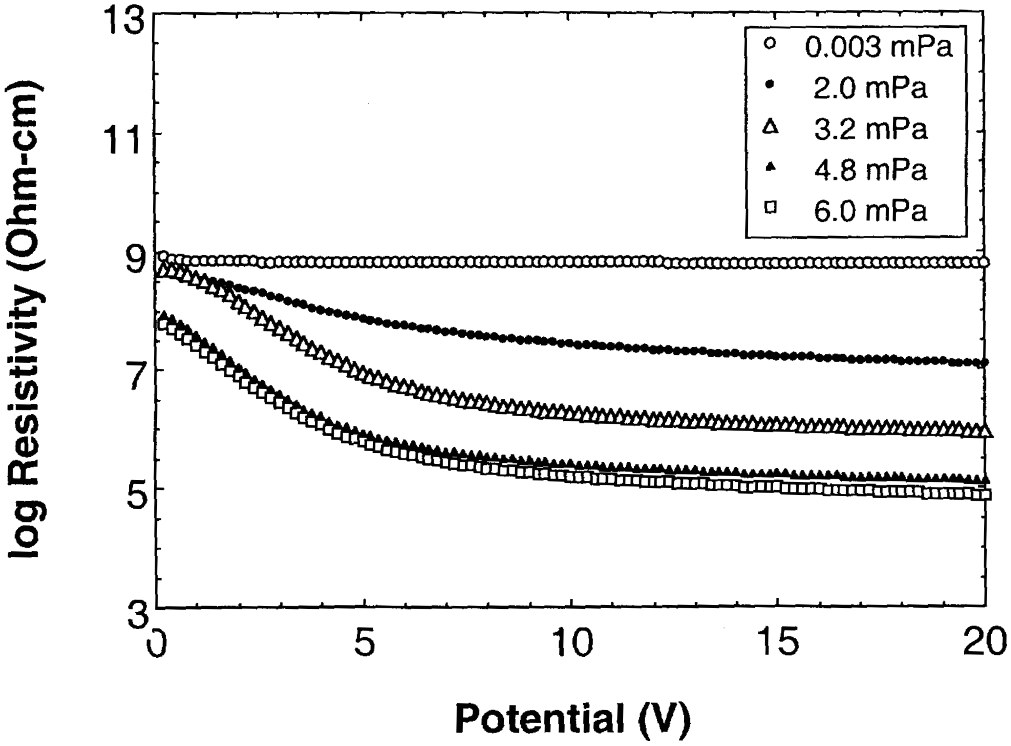

Figure 2. – The log variation of vertical resistivity ρ (Ohm-cm) with the applied potential (V) is plotted as measured for coatings deposited from the 7 wt.% TiO_2 target over a range of oxygen partial pressures up to 6 mPa in the working gas mixture.

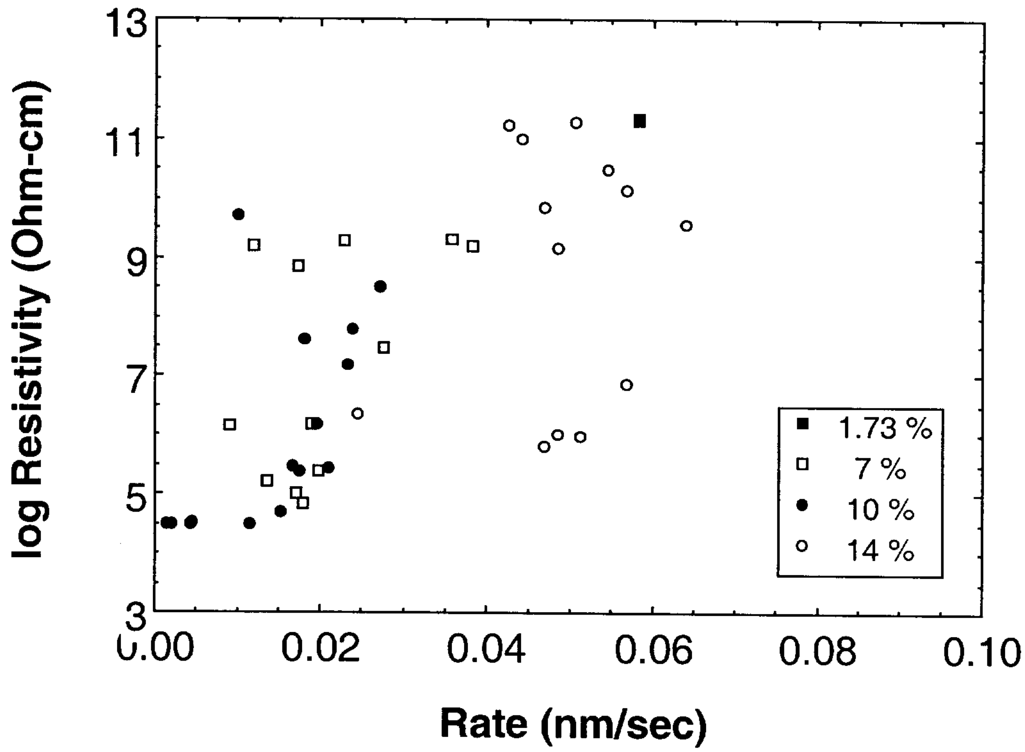

Figure 3. – The log variation of vertical resistivity ρ (Ohm-cm) in the coating with the deposition rate (nm sec^{-1}).

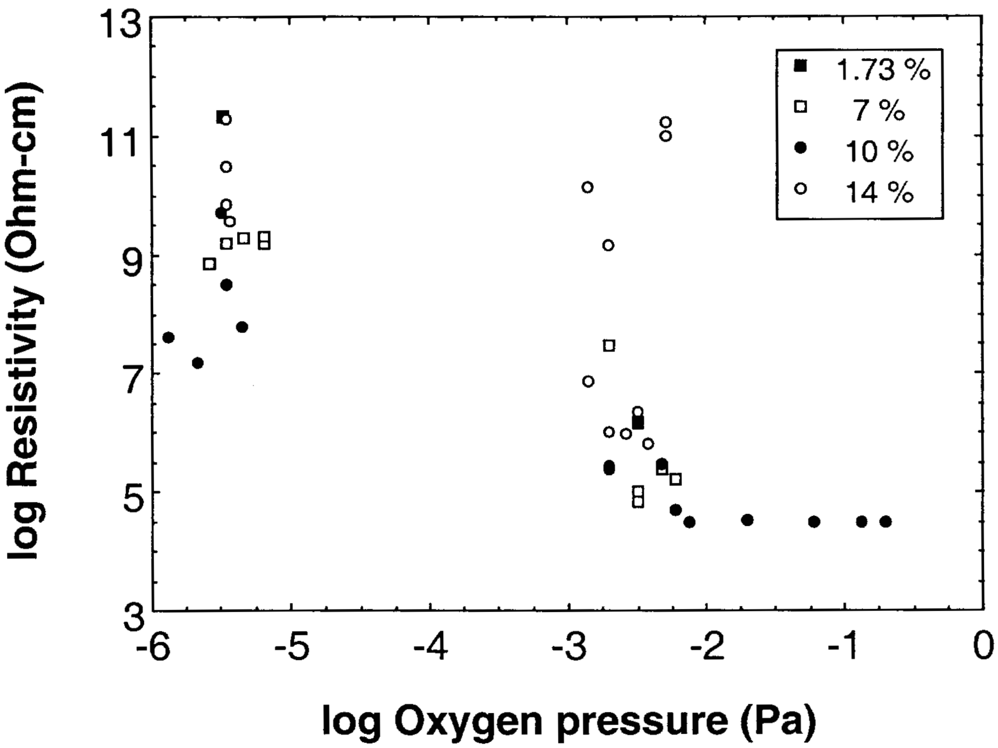

Figure 4. – The log-log variation of vertical resistivity ρ (Ohm-cm) in the coating with the partial pressure of oxygen (Pa) during the deposition.

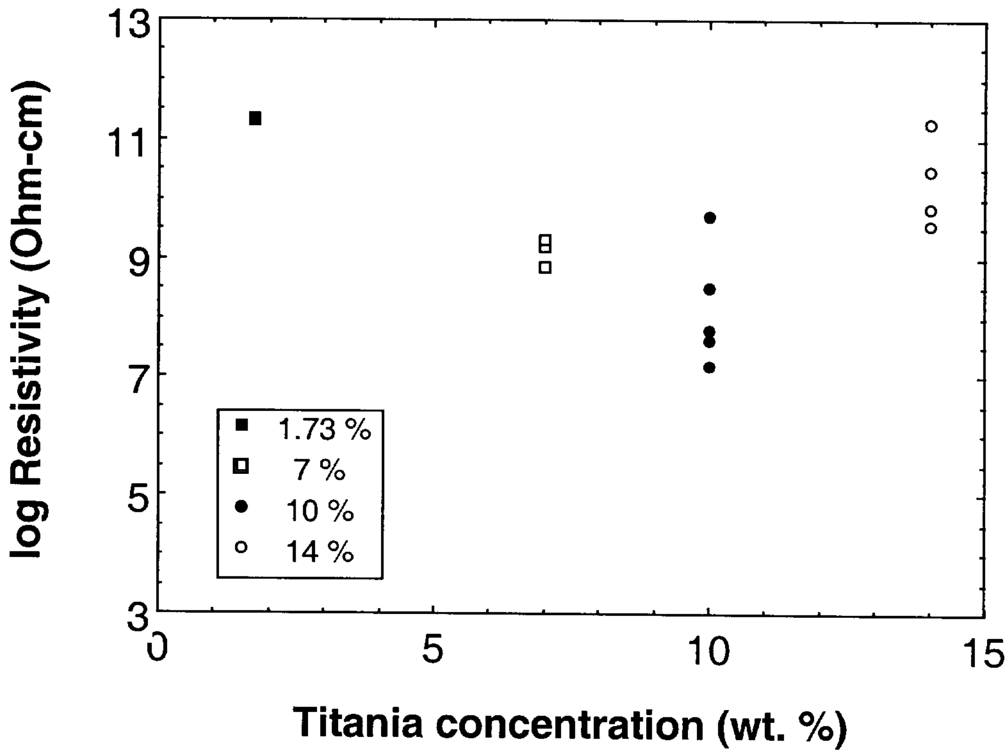

Figure 5. – The log variation of vertical resistivity ρ (Ohm-cm) in the coating with the TiO_2 content (wt.%) of the sputter target.

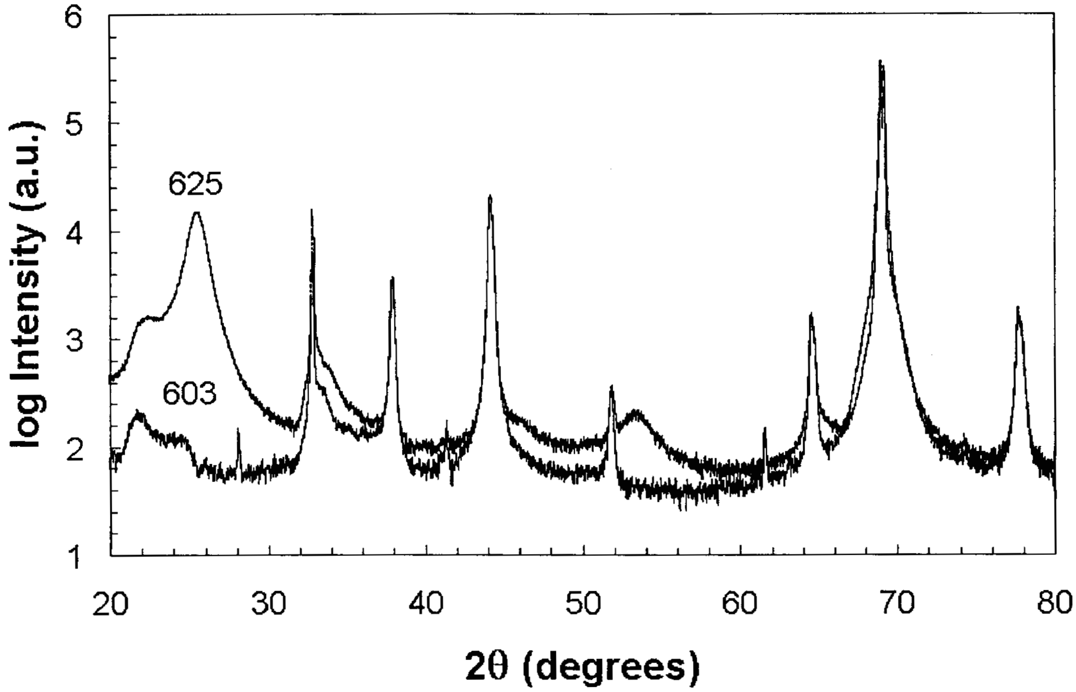

Figure 6. – The Cu $k\alpha$, $\theta/2\theta$ x-ray diffraction scans of the 7 wt.% TiO_2 coatings no. 603 and 625.